VELOCITY DISTRIBUTION IN AN INDUCTION PLASMA BY TRANSIENT TECHNIQUE

P. Meubus
Applied Sciences Department, University
of Quebec, Chicoutimi, P.Q., Canada
G7H 2B1

ABSTRACT

The gas velocity distribution in a R.F. argon plasma is found from data obtained during the transient regime of extinction. The time-intensity curves for the spectral lines 425.9 and 696.5 nm are used in order to obtain the transient temperatures. When the latter are used in conjunction with an energy balance equation, known limiting conditions for the gas velocity allow the equation to be solved for the gas velocity at time 0.

1. INTRODUCTION

Except for the measurement of electrons concentration in plasmas by means of interferometric measurements[1], transient conditions are seldom used for the purpose of diagnostics in plasma torches, at least to our knowledge. The present work shows how this particular regime in plasmas can be used for the determination of velocity distributions: significant velocity-containing terms are introduced in the energy balance and known velocity conditions are available at intermediate steps in the temperature decaying process, from which the initial gas velocity distribution can be derived. Since the duration of the transient process does extend to a number of milliseconds, local thermodynamic equilibrium is assumed, an assumption which is confirmed by the calculation of metastable species concentration, using absolute line emission 425.9 and 695.5 values.

2. EXPERIMENTAL

2.1 Apparatus

The set-up is shown on Fig. 1. The inductively heated plasma torch is generated from a 15 kw Hevi-Duty 5MHz generator. The spectroscopic part is a 1m focal length monochromator of the Czerny-Turner type, provided with a diffraction grating with 1180 groves/mm. The resolution is 0.11 nm at 310 nm. An EMI9558B photomultiplier, with maximum sensitivity around 500 nm, is followed by an amplifier and the spectroscopic signal is recorded on 15 MHz Hewlett-Packand oscilloscope.

The optical assembly is also shown of Fig. 1. The portion of interest of the plasma was projected on the screen shown, by means of a converging lens. A 2 mm diameter hole on the screen delineated the desired point on the plasma, where the reading was to be taken, the image of the screen hole being focused on the monochromator slit aperture.

2.2 Mode of operation

The torch was operated at atmospheric pressure. Central and peripheral argon without swirl velocity were injected in the torch up to a total of 20 000 cm^3/min, the central argon flow approximately cancelling out the upward gas velocity component due to the magnetohydrodynamic effects developed in the torch[2].

The velocity distribution was calculated, as an example of application of the method, at the lower outlet of the coupling antenna, at a distance z = 5.4 cm from the outlet L of the central upper probe. As developed later in the text, the velocity determination required the temperature-time curves during extinction of the plasma, so that the absolute intensity-time curves for spectral lines, which were chosen at 425.9 and 696.5 nm, were also determined for the transient conditions. These intensity-time curves were obtained by starting the plasma torch until stabilization was obtained, positioning the optical system to obtain laterally integrated intensity values throughout the circular section in the plasma at z = 5.4 cm , at given heights above the center, and then shutting off the power supply, the switch simultaneously triggering the oscilloscope. Figure 2 shows such curves obtained at various times for the 696.5 nm emission line in argon. Absolute radial intensity values were then obtained from these curves and a numerical calculation technique described by Nestor[3] was used for applying the Abel inversion method. Calibration of the optical and detection system was made by means of a 1000 W quartz iodine lamp (NBS standard of spectral irradiance). The peaks recorded on the oscilloscope for the spectral lines 425.9 and 696.5 nm were corrected for the corresponding spectral line surfaces by means of peak over line surface ratio calibrations.

3. RESULTS AND DISCUSSION

3.1 Temperature and L.T.E. conditions

From the preceding considerations, absolute radial power emission can be obtained for the spectral lines 425.9 and 696.5 nm, at z = 5.4 cm and a given temperature:

$$f(r)_{425.9} = \frac{n_m}{4\pi \times 10^7} \left[g \frac{A e^{-E/kT}}{\lambda} \right]_{425.9} hc/Q_T \qquad (1)$$

$$f(r)_{696.5} = \frac{n_m}{4\pi \times 10^7} \left[g \frac{A e^{-E/kT}}{\lambda} \right]_{696.5} hc/Q_T \qquad (2)$$

It is well known[4] that in low temperature plasmas (< 10 000K) for which the critical electrons concentration is not attained, argon metastables existing at the first excited levels ($1s_3$ and $1s_5$) may play the role of a fundamental level. The partition function Q_T in equations (1) and (2) was calculated using the $1s_3$ level at 11.55 eV as the reference fundamental level. The limiting principal quantum number was calculated from reference[5] and found equal to n = 13 in this case. Energy levels were obtained from Moore[6].

The temperature was determined by ascertaining a given value and calculating (1) and (2) until the values obtained for the total metastables n_m concentration were as close as possible. As shown in Fig. 3 the two values obtained for n_m are very close in each temperature case, thus indicating that accepta-

ble local thermal equilibrium did prevail during the temperature decay process shown in Fig. 4 as a function of radius and in Fig. 5 as a function of time. The concentration values obtained for the metastables between 4000 and 8000K, say between 10^{12} and 10^{13} per cm^3 are in agreement with data in the lite ratu-re[7]. Beyond 8000K, the fundamental level probably starts playing a role.

The temperatures in Fig. 4 were calculated from equations (1) and (2), using experimental data up to 1.3 cm and 8 ms. Extrapolated results were obtained from curve fitting:

$$T\Big|_{t\ =\ \text{constant}} = A_1 e^{b_1 r^2} \tag{3}$$

Figure (4) was then used to derive the curves in Fig. 5. One obtains:

$$T\Big|_{r\ =\ \text{constant}} = A_2 e^{b_2 t} \tag{4}$$

with a regression coefficient higher than 0.96 in both cases.

Results for A_1, A_2, b_1, b_2 and regression coefficient appear in Table 1.

3.2 Velocity determination

The temperature-time profiles shown in Fig. 5 converge toward a common temperature limiting value of 1500K (± 100K), at 18 ms, indicating a homogeneous temperature, which is the one assumed for the plasma, at least around the considered section, since $\frac{\partial T}{\partial z}$ is small, especially at the prevailing temperatures. This is the basis of the velocity distribution calculations at plane z = 5.4 cm. Since energy equipartition is obtained at any time during the temperature decaying period, an energy balance may be written, using cylindrical coordinates:

$$\frac{\partial (T\rho Cp)}{\partial t} + \frac{\partial (\rho Cp T v_z)}{\partial z} = \frac{1}{r}\frac{\partial}{\partial r}\left(rk\frac{\partial T}{\partial r}\right) - Q_R \tag{5}$$

Calculations show that second order axial heat diffusion terms and viscous effects may be neglected in equation (5) and swirl velocity is absent. The radiation term in argon has been evaluated[8]

$$Q_R = \frac{64\pi^{3/2}\,\varepsilon^6}{3\sqrt{6}m_e^{3/2}c^3}\ \frac{(Z^2 eff)}{\sqrt{T_e}}\ (n_e)^2\ \Delta\nu \tag{6}$$

Developing equation (5), one obtains, evaluated at a given r:

$$\frac{\partial T}{\partial t}\left(\rho Cp + Cp\ T\frac{\partial \rho}{\partial T} + \frac{\partial Cp}{\partial T}\rho T\right) = \frac{1}{r}\left(\frac{\partial k}{\partial T}\right)\left(\frac{\partial T}{\partial r}\right)^2 + \frac{k}{r}\frac{\partial T}{\partial r} + k\frac{\partial^2 T}{\partial r^2}$$
$$- C_p T v_z \frac{\partial \rho}{\partial z} - \rho T v_z \frac{\partial C_p}{\partial z} - \rho C_p T \frac{\partial v_z}{\partial z} - Q_R \tag{7}$$

When r is kept constant and the time increment δt is small enough, one can write, using the corresponding δz length around z = 5.4 cm:

$$\frac{\partial v_z}{\partial t}\,\delta t = \frac{\partial v_z}{\partial z}\,\delta z$$

or, taking limiting conditions:

$$\frac{\partial v_z}{\partial t}\,\frac{1}{v_z} = \frac{\partial v_z}{\partial z} \tag{8}$$

In the same way:

$$\frac{\partial T}{\partial z} = \frac{\partial T}{\partial t}\,\frac{1}{v_z}\,,\quad \frac{\partial C_p}{\partial z} = \frac{\partial C_p}{\partial t}\,\frac{1}{v_z}\,,\quad \frac{\partial \rho}{\partial z} = \frac{\partial \rho}{\partial t}\,\frac{1}{v_z}$$

Substituting these values in equation (7), one obtains:

$$\frac{\partial T}{\partial t}\left(\rho C_p + C_p T\,\frac{\partial \rho}{\partial T} + \rho T\,\frac{\partial C_p}{\partial T}\right) = \frac{1}{r}\left(\frac{\partial k}{\partial T}\right)\left(\frac{\partial T}{\partial r}\right)^2$$

$$+\,\frac{k}{r}\,\frac{\partial T}{\partial r} + k\,\frac{\partial^2 T}{\partial r^2} - C_p T\,\frac{\partial \rho}{\partial t} - \rho T\,\frac{\partial C_p}{\partial t} - \rho C_p T\,\frac{\partial v_z}{\partial t}\,\frac{1}{v_z} \tag{9}$$

All the terms in equation (9) can be evaluated from existing data for argon[9], Figs. 4 and 5 and equations (3), (4) and (6). As a result, a known value of $\frac{\partial v_z}{\partial t}\,\frac{1}{v_z}$ is obtained from equation (9) for a given pair of t and r values. Thus:

$$K_t = -\,\frac{1}{v_z(t)_r}\,\frac{\partial v_z}{\partial t}\bigg|_r \tag{10}$$

Also, a Taylor series development around $v_z(t)|_r$, taking δt small enough, yields:

$$v_z(t + \delta t)|_r = v_z(t)|_r + \frac{\partial v_z}{\partial t}\bigg|_r \delta t \tag{11}$$

or

$$v_z(t + \delta t)|_r = v_z(t)|_r - K_t v_z(t)|_r\,\delta t \tag{12}$$

At t = 18 ms a homogeneous temperature of 1500K (Fig. 5) is attained at any r and z = 5.4 cm and an average gas velocity of 1.00 m/s is obtained from the initial conditions.

Considering equation (10) and r = 0, an initial value is assumed for $v_z(0)|_{r=0}$ (at t = 0), so that:

$$v_z(0 + \delta t)|_{r=0} = v_z(0) - K_o v_z(0)|_{r=0}\,\delta t \tag{13}$$

δt being a chosen time increment. Subsequent values are then calculated until $0 + n\delta t = 18$ ms. If one then obtains $v_z(18)|_{r=0} = 1.00$ m/s the initial guess was correct. If this is not the case, an iteration process is used with

other initial velocity values until the correct one, or the actual velocity at r = 0 is obtained. The same method is used for obtaining the velocity at other r values. The final velocity distribution is shown on Fig. 6, this being an application example of the method at z = 5.4 cm.

An error calculation shows that the velocity found should bear an error of about 20%. Results are comparable with previous data obtained by other means[10,11].

NOMENCLATURE

A_1, A_2: constants in equations (3), (4), K,

b_1, b_2: constants in equations (3), (4), s^{-1}

c : velocity of light, $cm \cdot s^{-1}$

e : base of naperian log,

E : energy level, eV,

g : statistical weight,

h : planck constant, erg·s,

k : Boltzmann constant

K_t : constant in equation (8), s^{-1}

m : mass, g

n : particles concentration, cm^{-3}

C_p: specific heat $J \cdot g^{-1}$

Q_T: partition function

Q_R: radiation, $W \cdot cm^{-3}$

r : radius, cm,

T : temperature, K,

t : time, s

v_z: axial velocity, $cm \cdot s^{-1}$

$v_z(r)$: velocity at radius r

Z_{eff}: effective charge on ions. Here: 2.72

Greek letters

$\Delta\nu$: constant in equation (6), 1.45×10^{15}, s^{-1}

ε : electric charge, stat-coul,

λ : wavelength, nm

ρ : density, $g \cdot cm^{-3}$

Subscripts

e: pertaining to electrons

t: pertaining to time

r: pertaining to radius r

REFERENCES

1. D. Ashby, D.F. Jephcott, Appl. Phys. Letters, 3, 13 (1963).

2. T.B. Reed, Jl Appl. Phys., 32, 821 (1961)

3. O.H. Nestor, H.N. Olsen, SIAM Review, 2, 200 (1960)

4. D. Bourasseau, F. Cabannes, J. Chapelle, Astron. et Astrophys., 9, 339 (1970)

5. J.F. Bott, Phys., Fl. 8, (1966).

6. C.E. Moore, Atomic Energy Levels, NBS467, Vol. 1 (1949)

7. P. Ranson, J. Chapelle, J. Phys. 32, C5b-39-40 (1971)

8. H.E. Petschek, P.H. Rose, H.S. Glick, A. Kane, A.R., Kantrowitz, J. Appl. Phys. 26, 83 (1955)

9. H. Edels, J.D. Graggs, Prog. in Dielec., 6, 188 (1963)

10. M.J. Boulos, R. Gagné, R.M. Barnes, Can. Jl Chem. Eng., 3, 367 (1980)

11. P. Meubus, Can. Jl Che. Eng., 5, 616 (1974)

TABLE 1

CURVE FITTING FOR THE TEMPERATURE-RADIUS AND TEMPERATURE-TIME FUNCTIONS

FIGURE	VARIABLES		EQUATION CONSTANTS				REGRESSION COEFFICIENT
	TIME S	RADIUS cm	A_1 K	A_2 K	b_1 cm^{-2}	b_2 s^{-1}	
4*	0	0 to 1.3	9800		-0.21		0.96
	2	0 to 1.3	8640		-0.25		0.97
	4	0 to 1.3	6600		-0.18		0.98
	6	0 to 1.3	5600		-0.16		0.98
	8	0 to 1.3	4950		-0.27		0.97
5**	0 to 0.008	0		10250		- 90	0.98
	0 to 0.008	0.4		9400		-109	0.97
	0 to 0.008	0.8		8400		- 92	0.98
	0 to 0.008	1.3		6900		- 80	0.98

* Experimental values - Higher values for radius are extrapolated in Fig. 4.

** Deduced from Fig. 4 and extrapolated to 0.018s on Fig. 5.

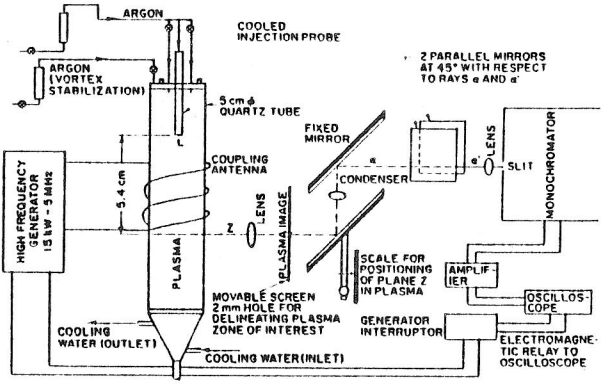

Fig. 1 Experimental set-up including optical assembly

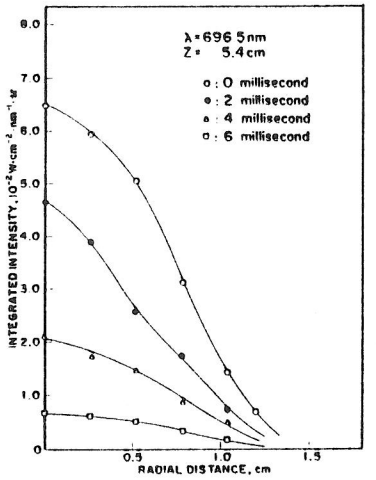

Fig. 2 Example of laterally integrated emission intensity for the spectral line 696.5 nm, at z=5.4cm

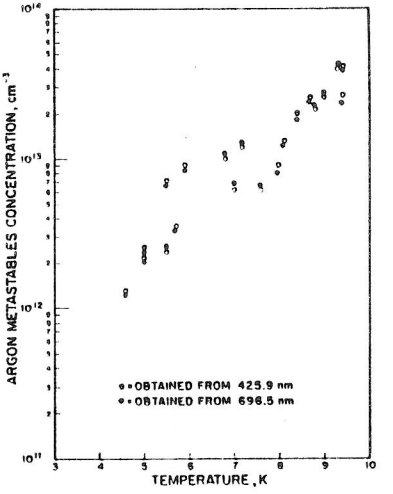

Fig. 3 Metastables concentration obtained from 425.9 and 696.5 lines. The closely situated points • and ∘ are, in all cases, related to a given temperature.

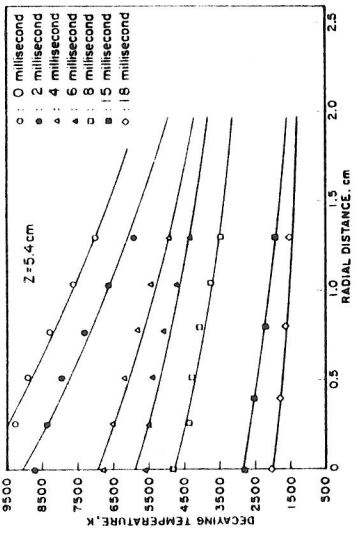

Fig. 4 Transient radial temperature curves. Experimental values: upto 8 ms and $0 \leq r \leq 1.3$ cm

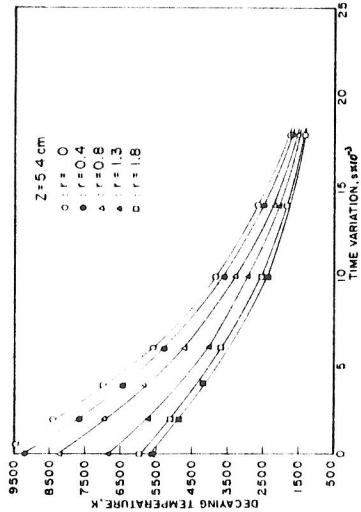

Fig. 5 Temperature-time curves for various radii. Derived from Fig. 4

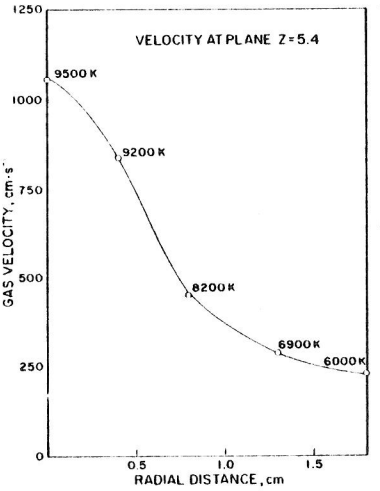

Fig. 6 Velocity distribution at z = 5.4 cm